Research Square

Preprints are preliminary reports that have not undergone peer review.
They should not be considered conclusive, used to inform clinical practice,
or referenced by the media as validated information.

Conductive Suppression of Piezoelectric Electromechanical Conversion in Fault-Zone Media

Andres Pech-Pérez
Universidad Autónoma Benito Juárez de Oaxaca
Magdalena Alvarado-Manzano
Colegio de Geofísicos
Carolina Romero-Salazar
Universidad Autónoma Benito Juárez de Oaxaca
Omar Augusto Hernandez-Flores
ohernandez.ciencias@uabjo.mx

Universidad Autónoma Benito Juárez de Oaxaca

Research Article

Keywords: piezoelectricity, fault-zone media, electromagnetic damping, dispersion relation, electrical conductivity, seismo-electromagnetics

Posted Date: June 30th, 2026

DOI: https://doi.org/10.21203/rs.3.rs-10132069/v1

License: This work is licensed under a Creative Commons Attribution 4.0 International License.
Read Full License

Additional Declarations: No competing interests reported.

Conductive Suppression of Piezoelectric Electromechanical Conversion in Fault-Zone Media

Andrés Pech-Pérez[1,2,3,4], Magdalena Alvarado-Manzano[2,3,4], Carolina Romero-Salazar[1], Omar A. Hernández-Flores[1*]

[1]Facultad de Sistemas Biológicos e Innovación Tecnológica, Universidad Autónoma Benito Juárez de Oaxaca, Av. Universidad S/N, Ex-Hacienda 5 Señores, Oaxaca de Juárez, 68120, Oaxaca, México.
[2]Smart Ray Geosolutions, Privada de Rosales 107, Col. Reforma, Oaxaca de Juárez, 68050, Oaxaca, México.
[3]Compañía de Optimización de Procesos en la Producción de Hidrocarburos, Calle Monrovia 907, Portales Sur, Alcaldía Benito Juárez, 03300, Ciudad de México, México.
[4]Colegio de Geofísicos, Av. Baja California 274 int. 2B, Col. Hipódromo Condesa, Alcaldía Cuauhtémoc, 06100, Ciudad de México, México.

*Corresponding author(s). E-mail(s): ohernandez.ciencias@uabjo.mx;
Contributing authors: andrespech@yahoo.com;
mag.alvaradomanzano@gmail.com; cromero.cat@uabjo.mx;

Abstract

Electromagnetic signals associated with seismic activity have been reported in different observational contexts, but their source mechanisms, amplitudes and reproducibility remain uncertain. Piezoelectric fault-zone models provide a useful analytical framework for relating elastic deformation to electric-field generation, although ideal formulations often neglect Ohmic dissipation in conductive rocks. Here, we extend a one-dimensional piezoelectric electromechanical model by introducing finite electrical conductivity into the coupled elastic–electromagnetic equations. The resulting complex dispersion relation is governed by the effective piezoelectric coupling $\boldsymbol{\Lambda}$, the elastic-to-electromagnetic velocity ratio $\boldsymbol{\alpha}$, and the conductive parameter $\boldsymbol{D}$. Asymptotic analysis and numerical root tracking show that the fast electromagnetic branch evolves from a weakly damped propagating

mode to an overdamped response as $\boldsymbol{D}$ increases. In contrast, for weak effective coupling and strong velocity separation, the slow mechanical branch remains close to the elastic dispersion relation. Nevertheless, the electric-field amplitude associated with the slow branch is suppressed by finite conductivity through a scale-dependent conversion factor. This suppression defines a critical conductivity and a dimensionless regime parameter that separate nearly lossless mechanical-to-electric conversion from Ohmic suppression. The results provide a compact analytical criterion for evaluating when piezoelectric electric fields generated by mechanical deformation can survive conductive attenuation in fault-zone media.

Keywords: piezoelectricity, fault-zone media, electromagnetic damping, dispersion relation, electrical conductivity, seismo-electromagnetics

1 Introduction

Electromagnetic anomalies associated with seismic activity have been reported in diverse tectonic settings over several decades, including geomagnetic perturbations, ultra-low-frequency emissions, atmospheric electric-field variations, ionospheric disturbances, and near-surface luminous phenomena (Johnston 2002; Zhao et al. 2022). Despite the variety of reported observations, their reproducibility remains limited, and their interpretation depends strongly on local geological, hydrological, and electrical conditions (Muto et al. 2006). This variability motivates physically grounded models that isolate specific coupling mechanisms between deformation and electromagnetic generation.

Among the proposed mechanisms, piezoelectricity in quartz-bearing rocks has long been considered a possible pathway for generating electric signals under mechanical stress (Finkelstein et al. 1973; Bishop 1981; Ogawa and Utada 2000; Wang 2021). The one-dimensional model of Wang (2021) provides a useful analytical framework because it separates the coupled electromechanical response into a fast electromagnetic branch and a slow mechanical branch. However, ideal piezoelectric formulations commonly assume lossless media, whereas natural fault-zone rocks have finite conductivity. This

limitation is important because conductivity controls not only current flow but also the attenuation and spatial persistence of electric fields (Hanekop and Simpson 2006).

The physical relevance of the fast electromagnetic branch has also been questioned under weak effective piezoelectric coupling (Yamazaki 2022). This critique reinforces the need to include realistic dissipative effects before assessing the possible geophysical significance of piezoelectric electromagnetic responses. In conductive crustal media, Ohmic currents modify the complex dispersion relation and can suppress the electric-field amplitude generated by mechanical deformation. Therefore, it is necessary to distinguish between local piezoelectric generation and the survival of the generated field over the relevant spatial scale.

Recent studies of seismo-electromagnetic phenomena and pressure-stimulated rock currents highlight the importance of considering generation, propagation, and attenuation within a unified physical framework (Surkov 2025; Mao et al. 2022; Xie et al. 2025). Motivated by this context, the present work extends the one-dimensional piezoelectric model by explicitly incorporating finite electrical conductivity. The analysis identifies the regimes in which piezoelectric conversion remains close to the lossless limit and those in which Ohmic dissipation dominates.

We show that conductivity affects the two coupled branches in different ways. The fast electromagnetic branch is directly damped by the conductive parameter and can become overdamped. In contrast, the slow mechanical branch remains nearly elastic in frequency under weak effective coupling, but the associated electric-field amplitude is reduced by a scale-dependent suppression factor. This distinction leads to a critical conductivity and a dimensionless regime parameter that provide a compact criterion for evaluating when piezoelectric electric fields generated by mechanical deformation can survive conductive attenuation in fault-zone media.

2 Conductive Piezoelectric Model

We consider a one-dimensional effective medium in which mechanical displacement $u(x,t)$ and electric field $E(x,t)$ are coupled through an effective piezoelectric coefficient. The model is not intended to represent the full three-dimensional geometry of a natural fault. It is a local linearized description of electromechanical coupling in a direction x. The strain and electric displacement are

$$\varepsilon = \mu^{-1}\sigma + \gamma E, \tag{1}$$

$$D_e = \gamma\sigma + \chi E, \tag{2}$$

where σ is stress, μ is elastic rigidity, γ is the effective piezoelectric coefficient, χ is permittivity and D_e is electric displacement. Since $\varepsilon = \partial u/\partial x$, the stress is

$$\sigma = \mu\frac{\partial u}{\partial x} - \mu\gamma E. \tag{3}$$

The equation of motion gives

$$\rho\frac{\partial^2 u}{\partial t^2} = \mu\frac{\partial^2 u}{\partial x^2} - \mu\gamma\frac{\partial E}{\partial x}, \tag{4}$$

where ρ is density and $v = (\mu/\rho)^{1/2}$ is the elastic wave speed. For harmonic solutions

$$u(x,t) = u_0 e^{i(\omega t - kx)}, \qquad E(x,t) = E_0 e^{i(\omega t - kx)}, \tag{5}$$

equation (4) gives

$$E_0 = \left(\frac{k^2 - \omega^2/v^2}{i\gamma k}\right) u_0. \tag{6}$$

This relation links the displacement amplitude to the electric-field amplitude and is one of the two algebraic relations used to obtain the dispersion equation.

The electromagnetic equation is obtained from Ampere's law with displacement current and Ohmic current. For a linear Ohmic medium, $\vec{J} = \eta\vec{E}$, where η is conductivity. In the one-dimensional effective geometry considered here,

$$\frac{\partial^2 E}{\partial x^2} = \zeta\eta\frac{\partial E}{\partial t} + \zeta\frac{\partial^2 D_e}{\partial t^2}, \tag{7}$$

where ζ is magnetic permeability. Using equations (2) and (3),

$$D_e = \gamma\mu\frac{\partial u}{\partial x} + \left(\chi - \gamma^2\mu\right) E. \tag{8}$$

Substitution of equation (8) and the harmonic fields into equation (7) yields

$$-k^2 E_0 = i\omega\zeta\eta E_0 - \frac{\omega^2}{c^2}\left(1 - \frac{\gamma^2\mu}{\chi}\right) E_0 + ik\omega^2\gamma\mu\zeta u_0, \tag{9}$$

where $c = 1/(\zeta\chi)^{1/2}$ is the effective electromagnetic wave speed. Eliminating E_0/u_0 between equations (6) and (9) gives

$$\left(1 - \frac{\gamma^2\mu}{\chi}\right)\omega^4 - ic^2\zeta\eta\,\omega^3 - (c^2 + v^2)k^2\omega^2 + ic^2v^2\zeta\eta k^2\omega + c^2v^2k^4 = 0. \tag{10}$$

Equation (10) is the conductive extension of the lossless piezoelectric dispersion relation. Terms proportional to η make the roots complex and therefore allow attenuation and relaxation to be analyzed explicitly.

3 Dimensionless Form and Branch Structure

The natural dimensionless variables are

$$\Omega = \frac{\omega}{ck}, \qquad \alpha = \frac{v^2}{c^2}, \qquad \Lambda = \frac{\gamma^2\mu}{\chi}, \qquad D = \frac{\zeta\eta c}{k} = \frac{\eta}{\chi ck}. \tag{11}$$

Using these variables, equation (10) becomes

$$(1-\Lambda)\Omega^4 - iD\Omega^3 - (1+\alpha)\Omega^2 + i\alpha D\Omega + \alpha = 0. \tag{12}$$

The conductive parameter $D = 1/Q_c$ compares Ohmic current with displacement current at the fast-mode scale $\omega_c = ck$. Thus, $D \ll 1$ indicates weak electromagnetic damping, whereas $D \gtrsim 1$ indicates that Ohmic currents are dynamically important. In crustal materials, $v \ll c$, so $\alpha \ll 1$, and effective piezoelectric coupling at rock scale is commonly weak, $\Lambda \ll 1$.

The names fast and slow branch refer to the phase velocities in the weak-coupling limit. They do not refer to the value of Λ itself. Setting $\Lambda = 0$, equation (12) factorizes as

$$(\Omega^2 - \alpha)(\Omega^2 - iD\Omega - 1) = 0. \tag{13}$$

The first factor gives $\Omega_- = \sqrt{\alpha}$, or $\omega_- = vk$, which is the slow mechanical branch. The second factor gives

$$\Omega_+ = \frac{iD + \sqrt{4 - D^2}}{2}, \tag{14}$$

which is the conductive fast branch. For $D \ll 1$,

$$\Omega_+ \approx 1 + \frac{iD}{2} - \frac{D^2}{8} + O(D^3). \tag{15}$$

The fast branch is then weakly damped. When D approaches order unity, damping becomes important; when $D \simeq 2$, the square root in equation (14) becomes purely imaginary and the asymptotic branch loses its real oscillatory component.

The slow branch has a different behavior. Equation (12) may be rewritten as

$$(\Omega^2 - \alpha)(\Omega^2 - iD\Omega - 1) = \Lambda\Omega^4. \tag{16}$$

This expression shows that the slow elastic factor communicates with the conductive electromagnetic factor only through finite piezoelectric coupling. A first-order perturbation around $\Omega_{s,0} = \sqrt{\alpha}$ gives

$$\delta\Omega_- \approx \frac{\Lambda\alpha^{3/2}}{2(\alpha - 1 - iD\sqrt{\alpha})}, \tag{17}$$

and hence, for $\alpha \ll 1$,

$$\frac{|\mathrm{Im}\,\Omega_-|}{|\mathrm{Re}\,\Omega_-|} \sim \frac{\Lambda D\alpha^{3/2}}{2(1 + D^2\alpha)}. \tag{18}$$

This correction is small in the weak-coupling and strong velocity-separation regime. Its maximum occurs when $D\sqrt{\alpha} \sim 1$, for which the relative damping is of order $\Lambda\alpha/4$. Therefore, conductivity does not substantially shift the slow-mode frequency under the conditions considered here. The important conductive effect for the slow branch appears instead in the conversion amplitude E_-/u_-.

Figure 1 summarizes this branch interpretation. The blue curve represents the real oscillatory part of the fast branch, which decreases as D approaches the overdamped threshold. The dashed red curve represents the magnitude of the fast-branch imaginary part, which increases with conductive damping. The black curve indicates that the slow branch remains close to $\Omega_-/\sqrt{\alpha} = 1$. Physically, the figure separates two effects that are often conflated: conductivity can destroy fast electromagnetic propagation, while the slow mechanical frequency can remain nearly elastic even though the generated electric field is attenuated.

4 Numerical Dispersion Maps

To verify the asymptotic interpretation, the complex roots of equation (12) were computed over logarithmic grids in D and α, with $\Lambda = 10^{-8}$ as a representative weak-coupling value. The positive-frequency fast branch was tracked by continuity, beginning at small D, where $\Omega_+ \approx 1$. The quantities mapped were $\mathrm{Re}(\Omega_+)$, $|\mathrm{Im}(\Omega_+)|$,

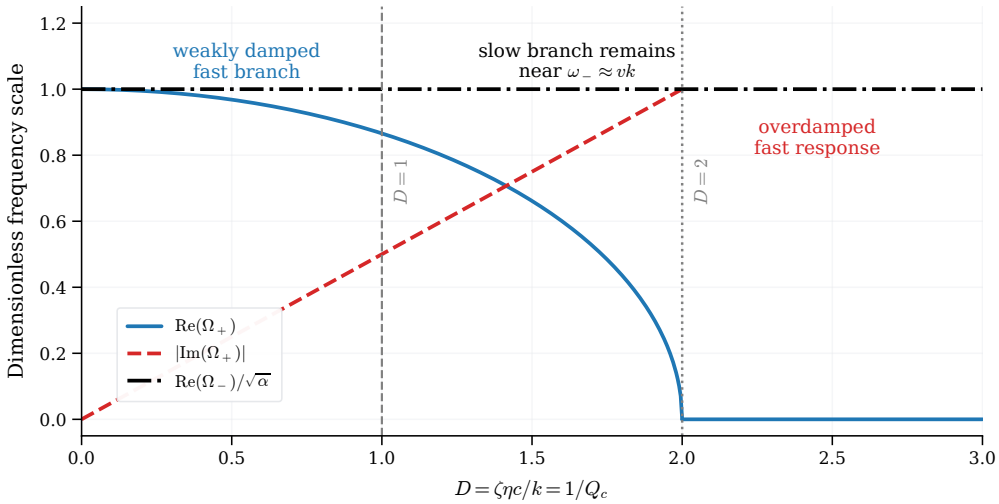


Fig. 1 Schematic asymptotic behavior of the fast and slow branches in the weak-coupling limit. The fast branch satisfies $\Omega_+ \approx (iD + \sqrt{4 - D^2})/2$, so for $D \ll 1$ it behaves as a weakly damped electromagnetic mode. Near $D \simeq 2$, the asymptotic fast branch loses its propagating character. In contrast, the slow branch remains close to $\Omega_- \approx \sqrt{\alpha}$, or $\omega_- \approx vk$, for weak effective piezoelectric coupling.

and the propagation index

$$P_+ = \frac{|\mathrm{Re}(\Omega_+)|}{|\mathrm{Re}(\Omega_+)| + |\mathrm{Im}(\Omega_+)|}. \tag{19}$$

Values $P_+ \approx 1$ indicate a predominantly oscillatory root, whereas $P_+ \approx 0$ indicates a relaxation-like or strongly attenuated response. The parameters used for the numerical maps are summarized in Table 1.

Figure 2 shows that the fast branch is controlled primarily by D, with only weak dependence on α over the explored range. Panel (a) shows that $\mathrm{Re}(\Omega_+)$ remains close to unity in the weakly conductive regime, consistent with the asymptotic expansion. Panel (b) shows that the imaginary component increases as D approaches order unity, signaling the onset of significant Ohmic attenuation. Panel (c) translates the complex-root structure into the propagation index P_+: the mode is propagating for $D \ll 1$, becomes mixed oscillatory–attenuated for $D \sim 1$, and approaches a non-propagating response near the overdamped limit. The physical meaning is that high conductivity

Table 1 Parameters used to generate the dispersion and slow-conversion maps. The high conductivities in the wavenumber cuts are illustrative and are used to display the conductive asymptotic regime.

Parameter	Symbol	Value or range	Use/meaning
Effective coupling	Λ	10^{-8}	Weak-coupling case
Conductive parameter	$D = \zeta\eta c/k$	10^{-4}–10^{4}	Fast-branch maps
Velocity ratio	$\alpha = v^2/c^2$	10^{-12}–10^{-6}	Fast-branch maps
Magnetic permeability	ζ	$4\pi \times 10^{-7}\,\mathrm{H\,m^{-1}}$	Non-magnetic medium
Effective permittivity	$\chi = \varepsilon_r\varepsilon_0$	$8.854 \times 10^{-11}\,\mathrm{F\,m^{-1}}$	$\varepsilon_r = 10$
Elastic wave speed	v	$3000\,\mathrm{m\,s^{-1}}$	Representative crustal speed
Elastic rigidity	μ	30 GPa	Representative rigidity
Conductivity range	η	10^{-10}–$10^{1}\,\mathrm{S\,m^{-1}}$	Suppression map
Selected wavelengths	λ	100 m, 1 km, 10 km, 100 km	Conductivity cuts
Selected conductivities	η	1, 10, 50, 100 $\mathrm{S\,m^{-1}}$	Wavenumber cuts

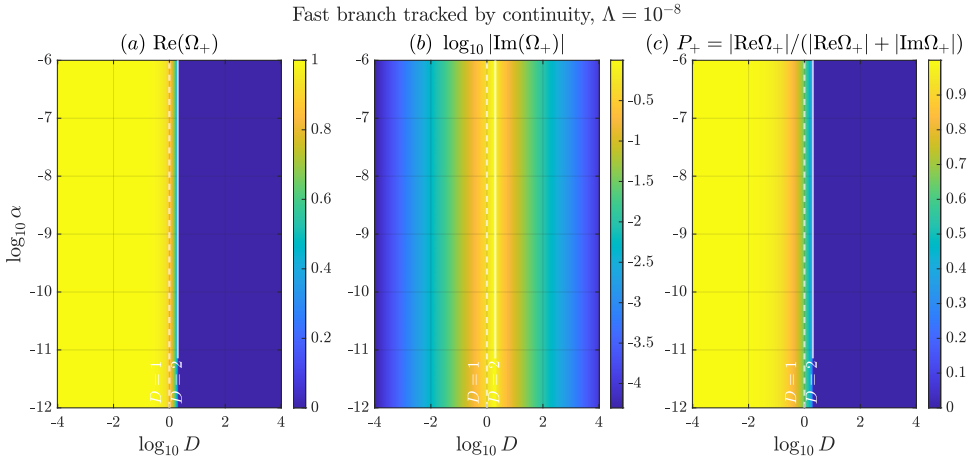


Fig. 2 Complex-root structure of the fast branch of the dimensionless conductive piezoelectric dispersion relation for $\Lambda = 10^{-8}$. The horizontal axis is $\log_{10} D$, where $D = \zeta\eta c/k = 1/Q_c$, and the vertical axis is $\log_{10}\alpha$, where $\alpha = v^2/c^2$. (a) Real part of the dimensionless fast-mode frequency. (b) Logarithm of the absolute imaginary part. (c) Propagation index P_+. The fast branch is weakly damped for $D \ll 1$, strongly attenuated for $D \sim 1$, and approaches an overdamped response near $D \simeq 2$.

or long wavelength can suppress the fast electromagnetic branch before it can behave as a coherent wave.

The slow branch behaves differently. Root tracking confirms that Ω_- remains close to $\sqrt{\alpha}$ for $\Lambda = 10^{-8}$. Its imaginary part is much smaller than its real part and follows equation (18). Thus, the dispersion maps support the interpretation that conductivity

strongly affects the fast electromagnetic branch, while the slow mechanical branch remains nearly elastic in frequency. The following section shows why this does not imply that the slow electric response is unaffected by conductivity.

5 Conductive Suppression of Slow Conversion

For the slow branch, the approximate conversion factor between mechanical displacement and electric field is

$$\frac{E_-}{u_-} \approx -\frac{ikv^2\gamma\mu\zeta}{p + i\frac{v\zeta\eta}{k}}, \tag{20}$$

where

$$p = 1 - \alpha(1 - \Lambda\alpha)(1 - \Lambda) \approx 1 \tag{21}$$

for $\alpha \ll 1$ and $\Lambda \ll 1$. The conductive term in the denominator is measured by

$$\mathcal{S} = \frac{v\zeta\eta}{k}. \tag{22}$$

The normalized slow conversion amplitude is

$$C_- = \frac{|E_-/u_-|}{|E_-/u_-|_{\eta=0}} = \frac{|p|}{\left[|p|^2 + \left(\frac{v\zeta\eta}{k}\right)^2\right]^{1/2}}, \tag{23}$$

and therefore, in the weak-coupling limit,

$$C_- \simeq \left[1 + \left(\frac{v\zeta\eta}{k}\right)^2\right]^{-1/2}. \tag{24}$$

Equation (24) is one of the main results of the study. It shows that the lossless slow conversion is recovered when $v\zeta\eta/k \ll 1$, whereas the electric-field amplitude is reduced

when $v\zeta\eta/k \gtrsim 1$. In the strongly conductive limit, $C_- \approx k/(v\zeta\eta)$. Conductivity therefore acts as a suppressive mechanism for the observable field amplitude, not as an amplification mechanism.

Using $k = 2\pi/\lambda$, the regime parameter becomes

$$\mathcal{S} = \frac{v\zeta\eta}{k} = \frac{v\zeta\eta\lambda}{2\pi} = \frac{\eta}{\eta_c}, \tag{25}$$

where

$$\eta_c \approx \frac{2\pi}{v\zeta\lambda}. \tag{26}$$

For $\eta \ll \eta_c$, the slow mechanical-to-electric conversion is nearly lossless. For $\eta \gtrsim \eta_c$, Ohmic suppression becomes important. Since $\eta_c \propto \lambda^{-1}$, long-wavelength perturbations are suppressed at lower conductivities than short-wavelength perturbations.

Figure 3 visualizes this criterion in the (η, λ) plane. The diagonal transition follows directly from $\mathcal{S} \propto \eta\lambda$. The lower-left region represents low conductivities and/or short wavelengths, where $\mathcal{S} \ll 1$ and $C_- \approx 1$. The upper-right region represents long wavelengths and/or high conductivities, where $\mathcal{S} \gg 1$ and $C_- \approx 1/\mathcal{S}$. The physical implication is that a conductivity value that is negligible at laboratory or short-wavelength scale can be important for long-wavelength fault-zone deformation.

Figure 4 shows the same physics in one-dimensional cuts. Panel (a) presents the normalized suppression in decibels as conductivity increases for selected wavelengths. The vertical threshold lines mark η_c, and their shift with λ illustrates that longer wavelengths enter the suppressed regime earlier. Panel (b) shows that, at fixed conductivity, suppression is strongest at small wavenumber. This is the spectral counterpart of the wavelength dependence in Figure 3. Together, Figures 3 and 4 show that the slow branch can remain mechanically elastic while its electric-field signature becomes difficult to observe in conductive media.

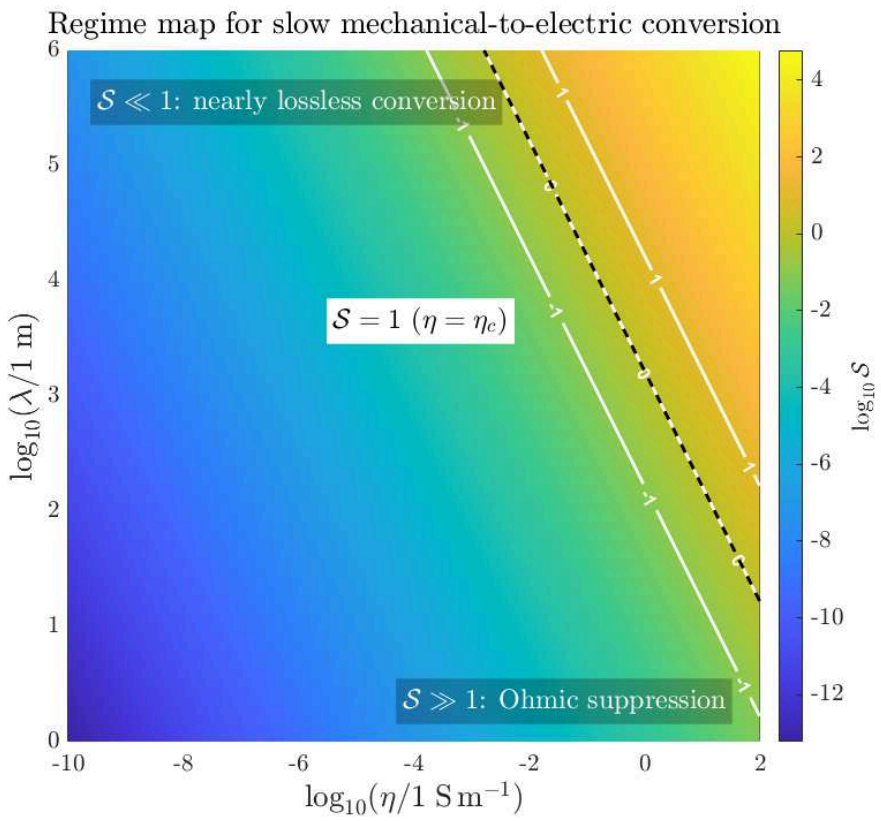


Fig. 3 Regime map for the slow mechanical-to-electric conversion. The color scale shows $\log_{10}\mathcal{S}$, where $\mathcal{S} = v\zeta\eta\lambda/(2\pi) = \eta/\eta_c$. The horizontal and vertical axes represent $\log_{10}(\eta/1\,\mathrm{S\,m^{-1}})$ and $\log_{10}(\lambda/1\,\mathrm{m})$, respectively. The contour $\mathcal{S} = 1$ separates nearly lossless conversion from Ohmic suppression.

6 Discussion

The conductive extension developed here clarifies the role of electrical conductivity in piezoelectric fault-zone models. In the lossless model, the fast and slow branches are real-frequency solutions that can be interpreted as predominantly electromagnetic and predominantly elastic modes. Once Ohmic conductivity is included, the roots become complex. This is not a minor mathematical detail: it determines whether a branch can behave as a propagating oscillatory response or as a strongly attenuated relaxation. For the fast branch, the transition is controlled mainly by $D = 1/Q_c$. When $D \ll 1$, displacement current dominates and the branch resembles a weakly damped

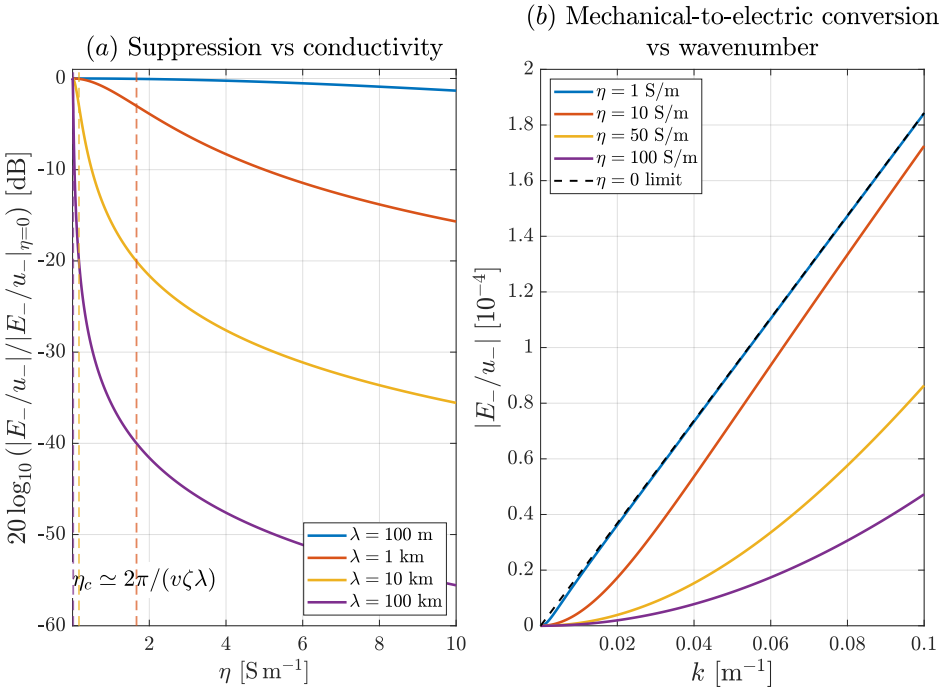


Fig. 4 Conductive suppression of the slow-branch mechanical-to-electric conversion factor. (a) Normalized suppression, $20\log_{10}(|E_-/u_-|/|E_-/u_-|_{\eta=0})$, as a function of electrical conductivity for selected wavelengths. Dashed vertical lines indicate $\eta_c \simeq 2\pi/(v\zeta\lambda)$. (b) Slow-branch conversion magnitude as a function of wavenumber for selected conductivities. Conductivity reduces the conversion efficiency, particularly at small wavenumbers.

electromagnetic wave. When $D \sim 1$, conduction current and displacement current are comparable. Near $D \simeq 2$, the leading-order fast root loses its real part and becomes overdamped.

The slow branch requires a different interpretation. The frequency of the slow branch remains close to $\omega_- = vk$ because its direct conductive damping is a higher-order effect in both Λ and α. This result might appear to suggest that conductivity is unimportant for the slow mechanically driven response. However, that conclusion would be incomplete. The observable electric field depends not only on the slow-mode frequency, but also on the conversion amplitude E_-/u_-. Conductivity enters that amplitude through the denominator in equation (20). Therefore, the slow branch can be mechanically robust while its associated electric field is Ohmically suppressed.

This distinction separates two physical questions. The first question is whether a fault-zone material has enough effective piezoelectric coupling to convert mechanical deformation into electric polarization. This is controlled by Λ, which depends on effective piezoelectric response, rigidity and permittivity. The second question is whether the generated electric response can survive conductive attenuation. This is controlled by $\mathcal{S} = v\zeta\eta\lambda/(2\pi)$. A small Λ reduces the absolute generated field, while a large $\mathcal{S}$ suppresses the field after generation. Both conditions must be considered when evaluating mechanically driven EM responses in fault-zone media.

The scale dependence of $\mathcal{S}$ has direct geophysical implications. For short wavelengths, such as laboratory-scale deformation or localized strain gradients, the critical conductivity η_c can be relatively high, allowing the lossless approximation to remain useful over a wider conductivity range. For long-wavelength deformation, η_c decreases, so the same material conductivity may produce substantial suppression. This provides a possible explanation for why piezoelectric conversion may be detectable under some conditions but ineffective under others, without requiring conductivity to play a contradictory role. Conductivity can support currents, but it also dissipates electric-field energy.

The model also places limits on interpretation. It does not predict earthquake lights or seismic EM precursors directly, and it should not be used as a standalone observational model. Natural fault zones are three-dimensional, heterogeneous, anisotropic and depth dependent. Conductivity, permittivity, elastic velocity and effective piezoelectric coupling may vary spatially and temporally as fractures open, fluids migrate, pore pressure changes and mineral alteration evolves. The present analysis should therefore be viewed as an analytical scaling framework for one local conversion stage. Future extensions should include finite source geometry, spatially variable electrical properties, anisotropic piezoelectric tensors, fracture networks, realistic boundary conditions and time-dependent mechanical forcing.

7 Conclusions

We extended a one-dimensional piezoelectric fault-zone model by including finite Ohmic conductivity. The dimensionless conductive dispersion relation is

$$(1-\Lambda)\Omega^4 - iD\Omega^3 - (1+\alpha)\Omega^2 + i\alpha D\Omega + \alpha = 0, \tag{27}$$

with $\Omega = \omega/(ck)$, $\Lambda = \gamma^2\mu/\chi$, $\alpha = v^2/c^2$, and $D = \zeta\eta c/k = 1/Q_c$. The main findings are as follows.

First, the fast electromagnetic branch is primarily controlled by D. It is weakly damped for $D \ll 1$, strongly attenuated for $D \sim 1$, and approaches an overdamped response near $D \simeq 2$. Second, the slow branch remains close to $\omega_- = vk$ for weak effective coupling and strong velocity separation, because its frequency damping scales as $\Lambda D\alpha^{3/2}/[2(1+D^2\alpha)]$. Third, conductivity suppresses the electric-field amplitude associated with the slow branch according to

$$C_- \simeq \left[1 + \left(\frac{v\zeta\eta}{k}\right)^2\right]^{-1/2}. \tag{28}$$

Fourth, the transition between nearly lossless conversion and Ohmic suppression is controlled by

$$\mathcal{S} = \frac{v\zeta\eta}{k} = \frac{v\zeta\eta\lambda}{2\pi} = \frac{\eta}{\eta_c}, \qquad \eta_c \approx \frac{2\pi}{v\zeta\lambda}. \tag{29}$$

Thus, finite conductivity does not amplify piezoelectric electric fields; it attenuates them. The lossless approximation remains valid only when $\mathcal{S} \ll 1$. Outside that regime, conductivity must be retained to assess whether mechanically generated piezoelectric electric fields can persist in fault-zone media.

Acknowledgements. The authors acknowledge financial support from CONAHCYT-SNI and the Universidad Autónoma Benito Juárez de Oaxaca.

Declarations

Funding. A. P-P. acknowledges the Sistema Nacional de Investigadoras e Investigadores, SNII, and the Secretaría de Ciencia, Humanidades, Tecnología e Innovación, SECIHTI, for financial support, and the Universidad Autónoma Benito Juárez de Oaxaca, UABJO, for granting access to its computer laboratories.

Conflict of interest. The authors declare that they have no conflict of interest.

Ethics approval and consent to participate. Not applicable.

Consent for publication. Not applicable.

Data availability. The data generated and analyzed in this study are available from the corresponding author upon reasonable request.

Code availability. The MATLAB scripts used to generate the dispersion and conversion maps are available from the corresponding author upon reasonable request.

Author contributions. All authors contributed to the conceptual development of the study. O. A. H-F. and A.P-P. developed the analytical formulation. O. A. H-F. Wrote the main manuscript and generated the numerical maps and figures. C. R-S and M. A-M. contributed to the physical interpretation and manuscript revision. All authors reviewed and approved the final manuscript.

References

Bishop, J.R.: Piezoelectric effects in quartz-rich rocks. Tectonophysics **77**(3–4), 297–321 (1981) https://doi.org/10.1016/0040-1951(81)90268-7

Finkelstein, D., Hill, R.D., Powell, J.R.: The piezoelectric theory of earthquake lightning. Journal of Geophysical Research **78**(6), 992–993 (1973) https://doi.org/10.1029/JC078i006p00992

Hanekop, O., Simpson, F.: Error propagation in electromagnetic transfer functions: what role for the magnetotelluric method in detecting earthquake precursors? Geophysical Journal International **165**(3), 763–774 (2006) https://doi.org/10.1111/j.1365-246X.2006.02948.x

Johnston, M.: Electromagnetic fields generated by earthquakes. In: International Geophysics vol. 81, pp. 621–635. Elsevier, Amsterdam (2002)

Muto, J., Nagahama, H., Miura, T., Arakawa, I.: Frictional discharge plasma from natural semiconductor/insulator junctions: origin of seismo-electromagnetic radiation. Physics and Chemistry of the Earth, Parts A/B/C **31**(4-9), 346–351 (2006) https://doi.org/10.1016/j.pce.2006.02.040

Mao, W., Wu, L., Xu, Y., Yao, R., Lu, J., Sun, L., Qi, Y.: Pressure-stimulated rock current as loading diorite to failure: Particular variation and holistic mechanisms. Journal of Geophysical Research: Solid Earth **127**, 2022–024931 (2022) https://doi.org/10.1029/2022JB024931

Ogawa, T., Utada, H.: Coseismic piezoelectric effects due to a dislocation 1: An analytic far and early-time field solution in a homogeneous whole space. Physics of the Earth and Planetary Interiors **121**(3–4), 273–288 (2000) https://doi.org/10.1016/S0031-9201(00)00177-1

Surkov, V.V.: An overview of theoretical studies of non-seismic phenomena accompanying earthquakes. Surveys in Geophysics **46**(1), 7–70 (2025) https://doi.org/10.1007/s10712-024-09869-1

Wang, J.-H.: Piezoelectricity as a mechanism on generation of electromagnetic precursors before earthquakes. Geophysical Journal International **224**(1), 682–700 (2021) https://doi.org/10.1093/gji/ggaa429

Xie, B., Wu, L., Sun, L., Xu, Y., Yoshikawa, A., Mao, W.: Mechanism of multiple anomalies prior to japan earthquakes from 2021 to 2023: Lithosphere-coversphere-atmosphere-ionosphere coupling driven by pressure-stimulated rock current. Earth and Space Science **12**, 2025–004320 (2025) https://doi.org/10.1029/2025EA004320

Yamazaki, K.: Comment on 'piezoelectricity as a mechanism on generation of electromagnetic precursors before earthquakes' by j. h. wang. Geophysical Journal International **228**(1), 792–795 (2022) https://doi.org/10.1093/gji/ggab372

Zhao, G., Zhang, X., Cai, J., Zhan, Y., Ma, Q., Tang, J., Du, X., Han, B., Wang, L., Chen, X., *et al.*: A review of seismo-electromagnetic research in china. Science China Earth Sciences **65**(7), 1229–1246 (2022) https://doi.org/10.1007/s11430-021-9930-5